J|A|C|S
ARTICLES
Published on Web 02/22/2006

Density Functional Theory and DFT+U Study of Transition Metal Porphines Adsorbed on Au(111) Surfaces and Effects of Applied Electric Fields

Kevin Leung,*,† Susan B. Rempe,† Peter A. Schultz,† Eduardo M. Sproviero,‡ Victor S. Batista,‡ Michael E. Chandross,† and Craig J. Medforth†

Contribution from Sandia National Laboratories, MS 1415, 1110, 0310, 1411, & 1349, Albuquerque, New Mexico 87185, and Department of Chemistry, Yale University, P.O. Box 208107, New Haven, Connecticut 06520-8107

Received September 27, 2005; E-mail: kleung@sandia.gov

Abstract: We apply density functional theory (DFT) and the DFT+U technique to study the adsorption of transition metal porphine molecules on atomistically flat Au(111) surfaces. DFT calculations using the Perdew−Burke−Ernzerhof exchange correlation functional correctly predict the palladium porphine (PdP) low-spin ground state. PdP is found to adsorb preferentially on gold in a flat geometry, not in an edgewise geometry, in qualitative agreement with experiments on substituted porphyrins. It exhibits no covalent bonding to Au(111), and the binding energy is a small fraction of an electronvolt. The DFT+U technique, parametrized to B3LYP-predicted spin state ordering of the Mn d-electrons, is found to be crucial for reproducing the correct magnetic moment and geometry of the isolated manganese porphine (MnP) molecule. Adsorption of Mn(II)P on Au(111) substantially alters the Mn ion spin state. Its interaction with the gold substrate is stronger and more site-specific than that of PdP. The binding can be partially reversed by applying an electric potential, which leads to significant changes in the electronic and magnetic properties of adsorbed MnP and ∼0.1 Å changes in the Mn−nitrogen distances within the porphine macrocycle. We conjecture that this DFT+U approach may be a useful general method for modeling first-row transition metal ion complexes in a condensed-matter setting.

I. Introduction

Metalloporphyrins (of which metal porphines are the simplest examples) are stable molecules which exhibit a wide range of optoelectronic, magnetic, and mechanical properties.[1] Deposited and/or self-assembled on metal electrodes, porphyrins are attractive candidates for novel molecular sensors,[2] memory,[3] and light-harvesting components.[4,5] Transition metal porphyrins are particularly interesting because of the multiple spin/electronic states available to them. For example, ligating the metal ions, or simply depositing the molecules on electrodes, can preferentially stabilize one state versus another. Understanding the detailed molecular interactions responsible for binding metalloporphyrins to well-characterized metal surfaces is therefore a subject of great technological interest, one which has received extensive experimental[2−12] and theoretical[13,14] study.

Memory and sensor applications of transition metal porphyrins rely on electrochemically induced switching of the electronic and magnetic states.[2,3] The field-dependent self-assembly and mobility of porphyrin molecules on electrodes have also been the subject of experimental interest under ultra-high-vacuum conditions[6] and in solution.[8,9] Electric-field-induced changes in the electronic states can lead to structural changes in porphyrin molecules, and this may impact their functions and reactivity in subtle ways.[15] Macrocycle conformational changes in nickel and zinc porphyrins have recently been the subject of a series of investigations.[16−18] Attaching ligands to Ni(II) or photoex-

† Sandia National Laboratories.
‡ Yale University.

(1) Kadish, K. M.; Smith, K. M.; Guilard, R. *The Porphyrin Handbook*; Academic Press: San Diego, 2000.
(2) Oni, J.; Diab, N.; Radtka, I.; Schuhmann, W. *Electrochim. Acta* **2003**, *48*, 3349.
(3) Gryko, D. T.; Clausen, C.; Roth, K. M.; Dontha, N.; Bocian, D. F.; Kuhr, W. G.; Lindsey, J. S. *J. Org. Chem.* **2002**, *65*, 7345.
(4) Imahori, H.; Norieda, H.; Yamada, H.; Nishimura, Y.; Yamazaki, I.; Sakata, Y.; Fukuzumi, S. *J. Am. Chem. Soc.* **2001**, *123*, 100. Nomoto, A.; Kobuke, Y. *Chem. Commun.* **2002**, 1104.
(5) Gust, D.; Moore, T. A.; Moore, A. L. *Acc. Chem. Res.* **2001**, *34*, 40.
(6) He, Y.; Ye, T.; Borguet, E. *J. Am. Chem. Soc.* **2002**, *124*, 11964.
(7) Yokoyama, T.; Yokoyama, S.; Kamikado, T.; Okuno, Y.; Mashiko, S. *Nature* **2001**, *413*, 619.
(8) Vesper, B. J.; Salaita, K.; Zong, H.; Mirkin, C. A.; Barrett, A. G. M.; Hoffman, B. M. *J. Am. Chem. Soc.* **2004**, *126*, 16653.
(9) Yoshimoto, S.; Inukai, J.; Tada, A.; Abe, T.; Morimoto, T.; Osuka, A.; Furuta, H.; Itaya, K. *J. Phys. Chem. B* **2004**, *108*, 1948.
(10) Kunitake, M.; Akiba, U.; Batina, N.; Itaya, K. *Langmuir* **1997**, *13*, 1607. Kunitake, M.; Batina, N.; Itaya, K. *Langmuir* **1995**, *11*, 2337.
(11) Hipps, K. W.; Scudiero, L.; Barlow, D. E.; Cooke, M. P. *J. Am. Chem. Soc.* **2002**, *124*, 2126.
(12) Yokoyama, T.; Yokoyama, S.; Kamikado, T.; Mashiko, S. *J. Chem. Phys.* **2001**, *115*, 3814.
(13) Lamoen, D.; Ballone, P.; Parrinello, M. *Phys. Rev. B* **1996**, *54*, 5097.
(14) Picozzi, S.; Pecchia, A.; Cheorghe, M.; Di Carlo, A.; Lugli, P.; Delley, B.; Elstner, M. *Surf. Sci.* **2004**, *566*, 628.
(15) Shaik, S.; de Visser, S. P.; Kumar, D. *J. Am. Chem. Soc.* **2004**, *126*, 11746.
(16) Song, Y.-J.; Haddad, R. E.; Jia, S.-L.; Hok, S.; Olmstead, M. M.; Nurco, D. J.; Schore, N. E.; Zhang, J.; Ma, J.-G.; Smith, K. M.; Gazeau, S.; Pécaut, J.; Marchon, J.-C.; Medforth, C. J.; Shelnutt, J. A. *J. Am. Chem. Soc.* **2005**, *127*, 1179.
(17) Gazeau, S.; Pécaut, J.; Marchon, J.-C. *Chem. Commun.* **2001**, 1644.
(18) Mazzanti, M.; Marchon, J.-C.; Shang, M. Y.; Scheidt, W. R.; Jia, S.-L.; Shelnutt, J. A. *J. Am. Chem. Soc.* **1997**, *119*, 12400.

citation can switch the low-spin nickel ground state with a $(d_{z^2})^2$ configuration to the high-spin expanded $(d_{z^2})(d_{x^2-y^2})$ state, so that core expansion causes the porphyrin ring to undergo a conformational change from a ruffled to a dome-like geometry. When outlying porphyrin appendages or bridles are attached to the Ni porphyrins, this small but energetic motion triggered by nickel spin state changes can potentially be harvested as nanomechanical motion in molecular switches.[16,17] It would be of great interest to extend this general principle to other transition metal porphyrins and related molecules deposited on gold electrodes. In such cases, the transition metal charge or spin states can be altered by electrochemical means, and the resulting conformational changes can be monitored using atomic force microscopy.

Given the wide range of interest in porphyrins adsorbed on metal surfaces, it is important to elucidate the precise nature of metalloporphyrin adsorption on and interaction with metal electrodes. Experimentally, it is known that certain substituted porphyrins and related molecules lie flat on Au(111) surfaces.[6−11] Even when they contain bulky substitutents, the molecules are only slightly distorted from a planar adsorption geometry.[12] It is also possible to have substituted porphyrins self-assembled into a tube-like geometry and lie edgewise on material surfaces if they are tethered using sulfide or other linkages.[4,8]

Density functional theory (DFT) might appear to be the theoretical method of choice to shed light on the binding energies, spin states, geometries, and external electric field effects of porphyrins adsorbed on metal surfaces. DFT simultaneously addresses the electronic and geometric properties of the composite molecule−metal system. It is a formally exact method, but the quality of its predictions depends on the approximate exchange correlation functional used. An early DFT calculation[13] was performed prior to detailed experimental studies of porphyrin adsorption on atomistically flat gold surfaces.[6,10−12] (For the purpose of this work, we ignore the herringbone surface reconstruction on Au(111),[19] which occurs on long length scales.) Motivated by molecular electronics experiments on self-assembled molecules which are somewhat similar to porphyrins,[20] Lamoen et al.[13] examined palladium porphines (PdP) adsorbed edgewise on Au(111) and reported a large (∼10 eV) binding energy. This calculation was performed using the local density approximation (LDA), which tends to overestimate the binding energy. A subsequent DFT work[14] considered PdP adsorbed in a similar edgewise geometry on Al(111) surfaces. This study reported a sub-electronvolt adsorption energy using LDA, and an even smaller binding energy was obtained using the Perdew−Burke−Ernzerhof (PBE)[21] version of the generalized gradient approximation (GGA) to the exchange correlation functional. GGA is generally more accurate than LDA for treating molecule−material binding[22] and has been widely used in such studies.[23]

Guided by recent experiments and building on these earlier DFT results, we set out to apply the PBE functional to re-examine PdP adsorption on the Au(111) surface as one of the goals of this work. We consider both the flat adsorption geometry found in experiments where porphyrins are not tethered to metal surfaces[6,10−12] and the edgewise geometry adopted in earlier calculations.

PdP can be considered a prototypical metalloporphyrin which adsorbs weakly on Au(111). For many transition metal compounds and materials, such as second-row elements like Pd, most implementations of DFT appear to yield the correct ground spin state and electronic properties, and they are valuable techniques to apply.[25] However, we are also interested in first-row transition metal porphyrins (e.g., Ni(II) and Mn(II), which are pertinent for studying effective ion size-driven conformational changes in porphyrin molecules).[16−18] Here we encounter a dilemma that has hindered DFT studies of composite systems involving first-row transition metal ions. In brief, DFT implementations with non-hybrid exchange correlation functionals such as PBE[21] and PW91,[24] widely used in the condensed matter physics community, treat gold and other metal surfaces accurately but are often less accurate for interactions between ligand/crystal field and first-row transition metal ions. The Becke three-parameter Lee−Yang−Parr (B3LYP)[26] hybrid exchange correlation functional correctly predicts the high-spin ground state for MnP but is, at present, too costly for modeling metal surfaces.[27,28]

Accurate predictions for bulk transition metals' lattice constants and magnetic properties were among the early successes of non-hybrid GGA.[29] PW91 and PBE are among this class of GGA. However, these functionals underestimate the exchange interaction among the strongly localized, partially filled 3d orbitals in first-row transition metal ions. This leads to underestimation of the stability of high-spin states in some first-row transition metal ions in impurity centers or ligand fields, where non-hybrid GGA often predicts ground states with incorrect spin multiplicities.[30−32] Indeed, a recent ab initio molecular dynamics simulation of Mn(II) centers was compelled to apply a high-spin constraint throughout the trajectory.[33]

Hybrid exchange correlation functionals contain fractional non-local or Hartree−Fock exchange, which amounts to 20% for B3LYP.[26] This admixture is apparently the right amount to reproduce the experimental spin ordering and energy splitting between spin states in many complexes between ligands and Mn,[34−36] as well as other first-row transition metal ions,[36] and is widely and successfully used for Mn centers.[34−39] A slightly

(19) Barth, J. V.; Brune, H.; Ertl, G.; Behm, R. J. *Phys. Rev. B* **1990**, *42*, 9307.
(20) Burghard, M.; Fischer, C. M.; Schmelzer, M.; Roth, S.; Hanack, M.; Göpel, W. *Chem. Mater.* **1995**, *7*, 2104.
(21) Perdew, J. P.; Burke, K.; Ernzerhof, M. *Phys. Rev. Lett.* **1996**, *77*, 3865.
(22) Moroni, E. G.; Kresse, G.; Hafner, J.; Furthmüller, J. *Phys. Rev. B* **1997**, *56*, 15629.
(23) Di Felice, R.; Selloni, A. *J. Chem. Phys.* **2004**, *120*, 4906.
(24) Perdew, J. P.; Wang, Y. *Phys. Rev. B* **1992**, *45*, 13244.
(25) Here the distinction between first- and second-row transition metal compounds specifically refers to the PBE deficiency in treating the coulomb repulsion between electrons strongly localized at the same site. For example, in Mott−Hubbard insulators, non-hybrid DFT have been described as deficient in this respect for f-electron compounds, high-T_c cuprates, and 3d (but not 4d) oxides (see ref 54, pp 205103−4).
(26) Becke, A. D. *J. Chem. Phys.* **1993**, *98*, 1372. Becke, A. D. *J. Chem. Phys.* **1993**, *98*, 5648. Lee, C. T.; Yang, W. T.; Parr, R. G. *Phys. Rev. B* **1988**, *37*, 785.
(27) See http://cms.mpi.univie.ac.at/vasp/ for preliminary benchmarks obtained using VASP version 5.
(28) Hybrid exchange correlation functionals with unscreened, long-range exchange terms may converge slowly with system size for metals and may be unsuitable for treating metal surfaces (Martin, R. L., private communications).
(29) See, e.g.: Singh, D. J.; Pickett, W. E.; Krakauer, H. *Phys. Rev. B* **1991**, *43*, 11628.
(30) Reiher, M.; Salomon, O.; Hess, B. A. *Theor. Chem. Acc.* **2001**, *107*, 48.
(31) Reiher, M. *Inorg. Chem.* **2002**, *41*, 6928.
(32) Leung, K. *Phys. Rev. B* **2002**, *65*, 012102.
(33) Ivanov, I.; Klein, M. L. *J. Am. Chem. Soc.* **2005**, *127*, 4010.
(34) Lundberg, M.; Siegbahn, P. E. M. *Phys. Chem. Chem. Phys.* **2004**, *6*, 4772.
(35) Lundberg, M.; Siegbahn, P. E. M. *J. Comput. Chem.* **2005**, *26*, 661.
(36) Koizumi, K.; Shoji, M.; Nishiyama, Y. M.; Maruno, Y.; Kitagawa, Y.; Soda, K.; Yamanaka, S.; Okumura, M.; Yamaguchi, K. *Int. J. Quantum Chem.* **2004**, *100*, 943.

smaller admixture yields better results in other cases.[30,31] At present, applying these hybrid functionals in simulation cells with periodic boundary condition is computationally costly—up to 100 times more so than for non-hybrid functionals.[27] This factor may further depend on system size. As such, B3LYP has seen only preliminary applications in condensed-phase systems.[40] To our knowledge, it has not been applied to the large, slab-like, periodically replicated supercells needed to study porphyrin adsorption on metal surfaces[28] or, for that matter, for large-scale DFT calculations that require periodic boundary conditions, such as in aqueous systems via ab initio molecular dynamics.[33] As will be shown, periodically replicated simulation cells with adequate Brillouin zone sampling are crucial for modeling porphyrin adsorption on gold surfaces.

We note that hybrid functionals are not universally successful for all transition metal species. For example, (1) hybrid functionals tend to overestimate the stability of $Ns^1(N-1)$-d^{n+1} electronic configurations over $Ns^2(N-1)d^n$ ones in transition metal atoms.[41] (So does non-hybrid GGA.[42]) This consideration does not play a role when the metal s-orbital is no longer available due to its involvement in doubly occupied bonding orbitals,[38] or in Mn(II)P and Mn(III)P, which have largely empty Mn 4s orbitals. (2) The binding energies and bond lengths of many transition metal dimers are more accurately predicted using non-hybrid rather than hybrid GGA.[42] This issue may be related to (1). Thus, complexes with Mn−Mn bonds may be particularly challenging for hybrid functionals.[43,44] (3) For as yet unknown reasons, B3LYP is ambiguous regarding the stability of the high-spin electronic configurations of some first-row transition metal porphines, such as ligated FeP,[45,46] while non-hybrid GGA performs considerably worse;[45] a larger admixture of Hartree−Fock exchange seems necessary in this case.

A promising alternative method to characterize the correct spin state is to use quantum Monte Carlo (QMC) methods, which up to now have been used to study porphine (H_2P) which lacks coordinated metal ions.[47] Another option is to impose the experimentally known spin polarization in the entire supercell.[33] As will be discussed, however, this approach may not yield accurate metal−nitrogen distances within the porphyrin ring. Furthermore, when a metal electrode is present, the bulk metal valence electrons can be excited to the conduction band to give arbitary spin multiplicities at negligible energy penalties. So, a global spin constraint will likely change the bulk metal magnetic behavior without affecting the adsorbed transition metal ion complex. Clearly, new computational techniques are needed to treat porphyrin molecules adsorbed on metals.

In this work, we apply the DFT+U method[48,49] to treat the composite manganese porphine−gold metal system. This method, which emphasizes the role of on-site screened coulomb interactions, has successfully predicted the correct electronic ground state for transition metal oxide crystals such as NiO[50] and $LaCoO_3$,[51] where traditional non-hybrid GGA has failed. This mean field approach augments the DFT exchange correlation interactons *among electrons in a subset of orbitals* (Mn 3d in our case) with Hartree−Fock-like interactions parametrized with coulomb (U) and exchange (J) terms. Electrons in these orbitals still interact with the rest of the system (including the C, H, and N atoms in the porphine ring and the Au(111) substrate) via the DFT formalism. The specific implementation we use is described in more detail in the Supporting Information.

Formally speaking, the parameters U and J are related to screened coulomb and exchange integrals.[50,52] In practice, U has been set at values required to achieve agreement with experiments.[53] When dealing with molecules embedded with transition metal ions, we propose that U and J can be fitted to either experiments or predictions via other gas-phase theoretical methods, such as high-level quantum chemistry, quantum Monte Carlo, and hybrid functional DFT—as long as the latter are known to agree with experiments. The DFT+U technique is readily amenable to periodically replicated simulation cells and is thus well suited for studying metal porphine molecules adsorbed on gold surfaces. We note that this method is empirical in nature, and it assumes that the correlation between the 3d electron can be approximated as static.[54] Nevertheless, it has seen wide and successful applications to many solid-state materials where LDA/GGA treatments fail for electronic/magnetic properties.[48,50,51,53] It may also become a general technique for ab initio molecular dynamics study of first-row transition metal centers in condensed phases.[33,55]

As a proof of principle, we will focus on a second prototype porphyrin: manganese(II) porphine (MnP). MnP exhibits behavior drastically different from that of PdP discussed above. PdP is umambiguously stable in the low-spin state, and PBE and DFT+U methods yield similar predictions. However, Mn(II) complexes in general and Mn(II) porphyrins in particular are known to have high-spin ground states.[56−58] We will show that PBE incorrectly predicts the intermediate-spin state to be the MnP ground state. On the other hand, by fitting U to B3LYP results (which yield the experimental high-spin ground state), both the high/intermediate spin energy splitting and the gas-phase MnP geometry are successfully reproduced using the DFT+U method.[59]

(37) Isobe, H.; Soda, T.; Kitagawa, Y.; Takano, Y.; Kawakami, T.; Shyoshioka, Y.; Yamaguchi, K. *Int. J. Quantum Chem.* **2001**, *85*, 34.
(38) de Visser, S. P.; Ogliaro, F.; Gross, Z.; Shaik, S. *Chem. Eur. J.* **2001**, *7*, 4954.
(39) Khavrutskii, I. V.; Musaev, D. G.; Morokuma, K. *Inorg. Chem.* **2003**, *42*, 2606.
(40) Prodan, I. D.; Scuseria, G. E.; Sordo, J. A.; Kudin, K. N.; Martin, R. L. *J. Chem. Phys.* **2005**, *123*, 014703 and references therein.
(41) Ricca, A.; Bauschlicher, C. W. *Chem. Phys. Lett.* **1995**, *245*, 150.
(42) Schultz, N. E.; Zhao, Y.; Truhlar, D. G. *J. Phys. Chem. A* **2005**, *109*, 4388 and references therein.
(43) Chai, J.-F.; Zhu, H.-P.; Stuckl, C. A.; Roesky, H. W.; Magull, J.; Bencini, A.; Caneschi, A.; Gatteschi, D. *J. Am. Chem. Soc.* **2005**, *127*, 9201.
(44) Sproviero, E. M.; Gascon, J. A.; McEvoy, J. P.; Brudvig, G. W.; Batista, V. S. *J. Biol. Inorg. Chem.* **2006**, in press.
(45) Ghosh, A.; Taylor, P. R. *Curr. Opin. Chem. Biol.* **2003**, *7*, 113. Ghosh, A.; Persson, B. J.; Taylor, P. R. *J. Biol. Inorg. Chem.* **2003**, *8*, 507.
(46) Ghosh, A.; Taylor, P. R. *J. Chem. Theory Comput.* **2005**, *1*, 597.
(47) Aspuru-Guzik, A.; el Akramine, O.; Grossman, J. C.; Lester, W. A. *J. Chem. Phys.* **2004**, *120*, 3049.
(48) Anisimov, V. I.; Zaanen, J.; Andersen, O. K. *Phys. Rev. B* **1991**, *44*, 943.
(49) Liechtenstein, A. I.; Anisimov, A. I.; Zaanen, J. *Phys. Rev. B* **1995**, *52*, 5467.
(50) Anisimov, V. I.; Kuiper, P.; Nordgren, J. *Phys. Rev. B* **1994**, *50*, 8257.
(51) Nekrasov, I. A.; Streltsov, S. V.; Korotin, M. A.; Anisimov, V. I. *Phys. Rev. B* **2003**, *68*, 235113.
(52) Pickett, W. E.; Erwin, S. C.; Ethridge, E. C. *Phys. Rev. B* **1998**, *58*, 1201.
(53) Rohrbach, A.; Hafner, J.; Kresse, G. *Phys. Rev. B* **2004**, *69*, 075413.
(54) Johannes, M. D.; Mazin, I. I.; Singh, D. J. *Phys. Rev. B* **2005**, *71*, 205103 and references therein.
(55) Asthagiri, D.; Pratt, L. R.; Paulaitis, M. E.; Rempe, S. B. *J. Am. Chem. Soc.* **2004**, *126*, 1285.
(56) Miller, J. C.; Sharp, R. R. *J. Phys. Chem. A* **2000**, *104*, 4889 and references therein.
(57) Kirner, J. F.; Reed, C. A.; Scheidt, W. R. *J. Am. Chem. Soc.* **1977**, *99*, 1093.
(58) Siegbahn, P. E. M. *Curr. Opin. Chem. Biol.* **2002**, *6*, 227.
(59) We have not conducted detailed studies of the MnP optical spectra or excited states predicted by the DFT+U technique. This will be the subject of future work.

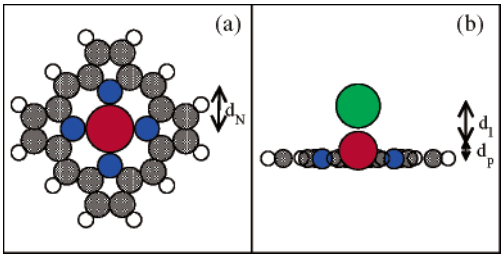

Figure 1. Metal porphine molecule, (a) without ligands and (b) attached to a ligand (Cl^- in this side view example). Carbon, nitrogen, hydrogen, metal, and chlorine atoms are depicted as gray, blue, white, red, and green circles, respectively. The metal−nitrogen (d_N), metal−porphine plane (d_p), and metal−ligand (d_l) distances are illustrated in the figure. As depicted, the metal ion in panel b is displaced toward the ligand atom, and d_p is defined as positive ("above the macrocycle ring"). The Au(111) substrate, if present, is below the macrocycle on the opposite side to the ligand.

Having validated the DFT+U technique for isolated MnP, we further apply it to investigate the geometric, electronic, and magnetic properties of MnP adsorbed on Au(111) surfaces. We also examine the effect of an electric field on the adsorbed MnP and show that it can induce significant changes in these properties. The MnP structure is particularly strongly affected by the applied field, with the Mn−N distance in the porphine ring increasing by up to 0.13 Å. This suggests that Mn porphyrins may exhibit conformational changes related to those seen for Ni porphyrins.[16]

To summarize, we have conducted a comprehensive study of the adsorption of two prototype transition metal porphine molecules, PdP and MnP, on gold surfaces. The effect of an applied electric field on the properties of adsorbed MnP is investigated. We also emphasize the success and importance of applying the DFT+U technique to treat the first-row transition metal ion Mn(II), and we conjecture that this technique may be widely applicable to condensed-phase systems.

This paper is organized as follows. Section II describes the methods and models used in our calculations. Section III details the results on isolated porphine molecules and porphines adsorbed on Au(111). Section IV concludes the paper with further discussion of the results obtained.

II. Methods and Models

DFT/PBE and DFT+U calculations are performed using the Vienna ab initio Simulation Package (VASP),[60] the projector augmented waves method,[61] and associated pseudopotentials.[62] For details of the DFT+U implementation, see Bengone et al.[63] and the Supporting Information. The cutoff for wave functions is set to 400 eV. LDA calculations are performed with both VASP and SeqQuest,[64] using ultrasoft pseudopotentials[65] and norm-conserving pseudopotentials, respectively. An energy convergence criterion of 10^{-3} eV for each atomic configuration is enforced.

Calculations on isolated porphyrin molecules (Figure 1) are performed using $16 \times 16 \times 10$ Å^3 simulation cells. For porphines with metal ions ligated with H_2O or Cl^- groups, cell sizes up to $16 \times 16 \times 15$ Å^3 are used, and dipole corrections are applied to remove the coupling between periodic images.[66−68] These simulation cells converge the spin splittings to 10 meV or better.

To model porphines deposited flat on Au(111) surfaces, we use supercells of lateral size 14.79×15.37 Å^2. They contain three to six gold layers of 30 Au atoms each, and we apply various Brillouin sampling schemes. The cell lengths in the z direction are 20, 22, 25, and 28 Å when three, four, five, and six layers of Au are present, respectively. The Au atoms in the bottom layer are fixed at their bulk face-centered-cubic (fcc) positions.[69,70] Dipole corrections are also applied for these slab geometry calculations.[66−68]

To study edgewise adsorption of PdP on Au(111) using LDA, we adopt the supercell of ref 13, except that the cell dimension in the z direction is increased to 27 Å to minimize the coupling between periodically replicated images. The supercell contains three gold layers, totaling 36 Au atoms, and a PdP molecule with two edge protons straddling a gold atom (see Figure 2b, below). The equilibrium PBE lattice constant is larger than that of LDA, and PBE investigations of this adsorption geometry employ a simulation cell of size $5.91 \times 15.36 \times 27$ Å^3. Monkhorst−Pack grids[71] of density up to $4 \times 2 \times 1$ are used to sample the Brillouin zone.

Optimizations and single-point energy calculations of gas-phase porphine molecules are computed with the program Jaguar[72] using the DFT B3LYP hybrid functional[26] with the 6-311G** basis set for second-row atoms, and the lacv3p** basis set for Mn that includes effective core potentials (ECPs).[73] Additional optimization calculations are performed using all-electron basis sets with the Gaussian 03 code.[74] Optimized energies are found with Ahlrichs and co-workers' all-electron TZV basis[75] on the metal ion and the 6-311G** basis for all other atoms, followed by a single-point energy calculation using the Wachters−Hay[76] all-electron basis set augmented with a diffuse d-function, 6-311+G, on the metal ion, and 6-31G* on all other atoms.

Molecular mechanics calculations are performed with the LAMMPS molecular dynamics software[77] modified to utilize the porphyrin potential reported by Shelnutt and co-workers.[78] The gold substrate is six layers thick and has dimensions 41 Å in the x and y directions. Au atoms are held fixed throughout the simulations; the gold−porphine interactions are calculated using previously published force fields.[79] Molecular mechanics total energy minimization calculations are converged to sub-millielectronvolt levels.

III. Results

A. Isolated Porphyrin Molecules. This section describes the geometries of isolated porphine molecules, and the energy splitting as a function of the spin multiplicity, as predicted by the different exchange correlation functionals. All symmetries are turned off in PBE and DFT+U calculations, which are performed using the VASP code and are converged to a few millielectronvolts. B3LYP calculations for MnP enforce D_{2h} or D_{4h} symmetry, depending on the Jahn−Teller distortion dictated by the degeneracy. Upon binding to a ligand or in the presence

(60) Kresse, G.; Furthmüller, J. *Phys. Rev. B* **1996**, *54*, 11169; *Comput. Mater. Sci.* **1996**, *6*, 15.
(61) Blochl, P. E. *Phys. Rev. B* **1994**, *50*, 17954.
(62) Kresse, G.; Joubert, D. *Phys. Rev. B* **1999**, *59*, 1758.
(63) Bengone, O.; Alouani, M.; Blöchl, P.; Hugel, J. *Phys. Rev. B* **2000**, *62*, 16392.
(64) Schultz, P. A. http://dft.sandia.gov/Quest.
(65) Vanderbilt, D. *Phys. Rev. B* **1990**, *41*, 7892.
(66) Neugebauer, J.; Scheffler, M. *Phys. Rev. B* **1992**, *46*, 16067.
(67) Bengtsson, L. *Phys. Rev. B* **1999**, *59*, 12301.
(68) Schultz, P. A. *Phys. Rev. B* **2000**, *60*, 1551.
(69) The PBE lattice constant for fcc gold is 4.182 Å, in good agreement with published lattice constants[70] computed using the PW91 exchange correlation functional.[24] PW91 is very similar to PBE used in this work; both overestimate the experimental lattice constant by 0.1 Å.
(70) Crljen, Z.; Lazić, P.; Sokcevic, D.; Brako, R. *Phys. Rev. B* **2003**, *68*, 195411.
(71) Monkhorst, H. J.; Pack, J. D. *Phys. Rev. B* **1976**, *13*, 5188.
(72) *Jaguar*, version 5.0; Schrodinger, LLC: Portland, OR, 2002.
(73) Russo, T. V.; Martin, R. L.; Hay, P. J. *J. Phys. Chem.* **1995**, *99*, 17085.
(74) Frisch, M. J.; et al. *Gaussian 03*, revision C.02; Gaussian Inc.: Wallingford, CT, 2004.
(75) Schaefer, A.; Horn, H.; Ahlrichs, R. *J. Chem. Phys.* **1992**, *97*, 2571.
(76) Wachters, J. H. *J. Chem. Phys.* **1970**, *52*, 1033. Hay, P. J. *J. Chem. Phys.* **1977**, *66*, 4377.
(77) Plimpton, S. *J. Comput. Phys.* **1995**, *117*, 1.
(78) Song, X.-Z.; Jaquinod, L.; Jentzen, W.; Nurco, D. J.; Jia, S.-L.; Khoury, R. G.; Ma, J.-G.; Medforth, C. J.; Smith, K. M.; Shelnutt, J. A. *Inorg. Chem.* **1998**, *37*, 2009. Shelnutt J. A.; Medforth C. J.; Berber M. D.; Barkigia, K. M.; Smith, K. M. *J. Am. Chem. Soc.* **1991**, *113*, 4077.
(79) Rappe, A. K.; Casewit, C. J.; Colwell, K. S.; Goddard, W. A., III; Skiff, W. M. *J. Am. Chem. Soc.* **1992**, *114*, 10024.

Table 1. Spin States and Relative Energies of Metal Porphines, and Some Intramolecular Distances: Metal−Nitrogen (d_N), Metal−Porphine Ring (d_p), and Metal−Ligand (d_l)[a]

porphyrin	method	E_{rel}	d_N	d_p	d_l	S
PdP	PBE	NA	2.035	0.000	NA	0
PdP	B3LYP	(0.000)	(2.043)	0.000	NA	0
PdP	B3LYP	(3.635)	(2.121)	0.000	NA	1
PdTPP[b]	expt.	NA	2.009	0.000	NA	0
PdOEP[c]	expt.	NA	2.018	0.000	NA	0
MnP	PBE	0.000	2.003	0.000	NA	3/2
MnP	PBE	0.495	2.051	0.000	NA	5/2
MnP	DFT+U	0.233	2.011	0.000	NA	3/2
MnP	DFT+U	0.000	2.090	0.000	NA	5/2
MnP	B3LYP	0.190	2.015	0.000	NA	3/2
MnP	B3LYP	(0.247)	(2.011)	0.000	NA	3/2
MnP	B3LYP	0.000	2.090	0.000	NA	5/2
MnP	B3LYP	(0.000)	(2.089)	0.000	NA	5/2
MnTPP[d]	expt	NA	2.085	0.000	NA	5/2
Mn(H_2O)P	PBE	NA	2.013	0.024	2.39	3/2
Mn(H_2O)P	DFT+U	NA	2.108	0.129	2.34	5/2
MnClP	PBE	0.492	2.014	0.255	2.17	1
MnClP	PBE	0.000	2.036	0.246	2.31	2
MnClP	DFT+U	0.545	2.040	0.278	2.28	1
MnClP	DFT+U	0.000	2.045	0.267	2.31	2
MnClTPP[e]	expt	NA	2.001	0.156	2.296	2

[a] Only the ground state of Mn(H_2O)P is tabulated. Energies and distances are in units of eV and Å, respectively. B3LYP results with/without parentheses are computed using different basis sets (see text). Experimental results in the solid phase: [b]tetraphenylporphinatopalladium(II) (PdTPP),[85] [c]octaethylporphinatopalladium(II) (PdEOP),[86] [d]tetraphenylporphinatomanganese(II) (MnTPP),[57] and [e]tetraphenylporphinatomanganese(III) chloride (MnCTPP).[84] NA, not applicable.

of a substantial electric field, the metal ion is displaced out of the porphine ring toward the ligand atom by a distance d_p, where the porphine ring position is taken to be the average z coordinate of the 36 porphine atoms excluding the metal ion. The distance between the transition metal ion and the ligand atom closest to it is defined as d_l. These definitions are illustrated in Figure 1.

Table 1 shows that B3LYP predicts a high-spin ($S = 5/2$) ground state for MnP, more stable by 0.21 (0.25) eV than the intermediate-spin state ($S = 3/2$). The values without/with parentheses are computed using the all-electron (TZV/6-311G**//6-311+G/6-31G*) basis set, or lacv3p** (Mn) and 6-311G** (other atoms), respectively. They show that neither the high spin−intermediate spin energy splitting nor the molecular geometry is strongly affected by the basis set used. (We have listed the average of the two Mn−N distances in the case of quartet MnP, which has a D_{2h} symmetry.) The stability of the high-spin state is in agreement with experiments on substituted manganese porphyrins.[56] PBE, on the other hand, incorrectly predicts that $S = 3/2$ is more stable than $S = 5/2$ by ~0.50 eV. When we set $U = 4.2$ eV, $J = 1.0$ eV within the DFT+U approach, the $S = 5/2$ spin-polarized state becomes more stable than the $S = 3/2$ state by 0.23 eV. This is sufficiently close to the B3LYP results for our purpose.[80,81] Since DFT+U predicts that all Mn(II)P and Mn(III)P species examined in this work are high spin, these ground-state predictions are not affected by spin contamination.[82] We emphasize that we use B3LYP as a standard to parametrize our DFT+U work because it yields the correct high-spin ground state for MnP;[57] as discussed in the Introduction, B3LYP is not universally successful for all transition metal compounds.

With these parameters, the ground-state Mn−N distance is predicted to be $d_N = 2.090$ Å, very similar to the B3LYP prediction and within 0.005 Å of the experimental value of 2.085 Å measured for the corresponding tetraphenylporphyrin derivative.[57] On the other hand, even when the total spin is constrained to $S = 5/2$, PBE predicts a Mn−N distance of 2.051 Å, or 0.034 Å smaller than the experimental value. Thus, even with a high-spin constraint, PBE underestimates Mn−N distances in Mn(II)P, while the DFT+U approach can be parametrized to yield both the correct spin state and a reasonable metal−porphine geometry.

Attaching a H_2O ligand to Mn does not qualitatively change the above analysis, with PBE still predicting an incorrect $S = 3/2$ spin state and a Mn−N distance substantially smaller than that predicted using the DFT+U method.

The energy splitting between the high- and intermediate-spin states is sensitive to U, while the Mn−N distance is less sensitive. For example, setting $U = 3.8$ eV instead of 4.2 eV yields a 0.12 eV splitting, but the Mn−N bond length remains essentially unchanged at 2.088 Å.

In MnPCl, spectroscopic measurements have confirmed that Mn is in the high-spin Mn(III) oxidation state,[83] in agreement with DFT+U and PBE predictions. These methods also predict similar Mn−N bond lengths that overestimate the experimental value in substituted porphyrins by up to 0.04 Å.[83,84] This discrepancy may be related to the ~0.1 Å difference in the predicted and measured out-of-plane Mn displacement. In the gas phase, the predicted change in Mn−N distance between the Mn(III) and Mn(II) oxidation states is thus underestimated. Despite this, as will be seen, DFT+U predicts a significant increase in this bond length when Mn(III)P adsorbed on Au(111) is switched to a Mn(II)-like oxidation state with an electric field.

PBE predicts that PdP is low spin, $S = 0$, in agreement with experiments.[87,88] So does DFT+U (not shown). In general, the 4d electrons in second-row transition metal ions are less localized than 3d electrons in first-row transition metal ions, and non-hybrid GGA methods such as PBE appear more reliable in predicting the ordering of their spin states than is the case with 3d electron systems.[25]

B. Normal-Coordinate Structural Decomposition. The conformations of the porphine macrocycles in the predicted structures are further examined using normal-coordinate structural decomposition (NSD).[89] NSD has emerged as a useful method for analyzing deformations of tetrapyrrole macrocycles in heme proteins and in synthetic proteins,[90] and such analyses

(80) Kozlowski et al.[81] pointed out that, even when using the *same* functional, localized basis Gaussian and plane-wave-based calculations can yield discrepancies in the low-/intermedate-spin splittings. This may be a pseudopotential effect. But the two methods are in agreement on the intermediate-/high-spin splitting, which is what we use to fit DFT+U parameters. Using plane-wave basis VASP calculations, we have reproduced Kozlowski et al.'s local basis PW91-predicted splittings in Fe(II)P to within 0.04 eV.

(81) Kozlowski, P. M.; Spiro, T. G.; Bérces, A.; Zgierski, M. Z. *J. Phys. Chem. B* **1998**, *102*, 2603.

(82) Furthermore, the gas-phase B3LYP results for intermediate- and low-spin states show negligible spin contamination, and the DFT+U geometries for these are similar to B3LYP predictions.

(83) Boucher, L. J. *Coord. Chem. Rev.* **1972**, *7*, 289 and references therein.

(84) Cheng, B.; Scheidt, W. R. *Acta Crystallogr. C* **1996**, *52*, 361.

(85) Fleischer, E. B.; Miller, C. K.; Webb, L. E. *J. Am. Chem. Soc.* **1964**, *86*, 2342.

(86) Ishii, T.; Aizawa, N.; Yamashita, M.; Matsuzaka, H.; Kodama, T.; Kikuchi, K.; Ikemoto, I.; Iwasa, Y. *J. Chem. Soc., Dalton Trans.* **2000**, *23*, 4407.

(87) Seo, J.-C.; Chung, Y.-B.; Kim, D. *Appl. Spectrosc.* **1987**, *41*, 1199 and references therein.

(88) Singh, A.; Johnson, L. W. *Spectrochim. Acta A* **2003**, *59*, 905 and references therein.

(89) Jentzen, W.; Song, X.-Z.; Shelnutt, J. A. *J. Phys. Chem. B* **1997**, *101*, 1684.

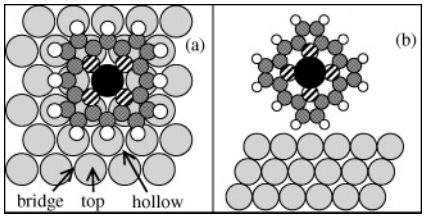

Figure 2. Palladium porphine on Au(111). (a) Flat adsorption geometry, with Pd on the top site. The top, hollow, and bridge sites are illustrated. (b) Edgewise adsorption. Striped circle, N; black, Pd; dark gray, C; white, H; light gray, Au. Periodic boundary conditions are used in all three directions (a vacuum layer separates the gold surfaces); only the gold atoms in the primitive simulation cell are shown. For the geometry in (b), the porphine molecules are in fact self-assembled in a tube-like stack along the gold surface.

are pertinent to the potential use of transition metal porphyrins adsorbed on metal electrodes as conformational switches.[16,17] Complete NSD analyses of selected structures from Table 1 are given in Tables S4−S13 of the Supporting Information. The PBE-predicted structure for PdP and DFT+U-predicted ones for MnP and MnClP show negligible amounts (less than 0.03 Å) of nonplanar deformation, consistent with the crystallographic data for other transition metal porphines (see Table S13). For comparison, highly substituted and very nonplanar porphyrin macrocycles exhibit up to 4 Å deformations in the soft ruffling (B_{1u}) or saddling (B_{2u}) modes.[91]

NSD also provides details of the in-plane deformations present in the isolated porphine macrocycles.[89] In-plane deformations are not usually analyzed in any detail because they are naturally intertwined with out-of-plane deformations in substituted porphyrins,[91] making it difficult to isolate the former. However, in the case of the porphines where the macrocycles are all nominally planar, it is possible to see the in-plane deformations resulting from the changes in the size of the metal complexed to porphine. For example, in the structures of PdP (PBE), MnClP (DFT+U), and MnP (DFT+U), the metal−nitrogen distances are 2.035, 2.045, and 2.090 Å, respectively. (The X-ray structure of nickel(II) porphine exhibits an even smaller metal−nitrogen distance of 1.951 Å because of the small size of the Ni(II) ion; see Table S13.) The NSD studies reveal a corresponding increase in the first-order A_{1g} (breathing) deformation as the porphine ring expands to accommodate the larger metal ion. The first-order A_{1g} deformations are +0.15, +0.11, and +0.37 Å (and −0.16 Å for NiP). Finally, we note that the discrepancy between the metal−nitrogen distances predicted for PdP and measured in PdTPP and PdOEP may be related to the in-plane deformations that accompany the out-of-plane deformations in the latter, as the crystal structures of these Pd complexes adopt nonplanar conformations of the type that are known to shorten the metal−nitrogen bond[78] (e.g., the large ruffling (B_{1u}) out-of-plane deformation in PdTPP (see Table S5)).

C. Palladium(II) Porphine on Au(111). We consider two adsorption geometries: a flat adsorption geometry suggested by experiments on substituted porphyrins[6,10−12] (Figure 2a) and the edgewise porphyrin stack configuration examined in ref 13, with successive macrocycles separated by ∼5.9 Å (Figure 2b).

1. Edgewise Adsorption. When we attempt to adsorb PdP on Au(111) in the edgewise geometry depicted in Figure 2b using the PBE exchange correlation functional, we find little or no attraction between the PdP tube and the gold substrate. In fact, PBE even predicts that the PdP molecules repel each other when they reside 5.91 Å apart in the self-assembled tube-like geometry in the *absence* of gold. The formation energy of this PdP tube is +0.06 eV when using 4 × 2 × 1 Brillouin zone sampling. The small repulsion is partly due to the fact that PBE underestimates van der Waals attractions. Surprisingly, we find that the Γ-point Brillouin zone sampling used in refs 13 and 14 yields an (unconverged) 0.31 eV repulsion. This is despite the fact that there is at most a 0.04 eV dispersion in the PdP valence electron states near the Fermi level. Regardless of which PdP reference energy is used—the isolated porphine or porphine tube—we find no attractive interaction between PdP and Au(111), in contrast to the ∼10 eV binding energy previously reported by Lamoen et al.[13]

Lamoen et al. applied LDA, not the PBE exchange correlation functional. They reported that the closest distance between PdP edge protons and a Au atom is 1.78 Å, suggesting a strong covalent bond between H and Au. The large adsorption energy was rationalized by comparing this system with the interaction of hydrogen molecules on transition metal surfaces.[13] While LDA is known to predict overbinding of molecules on metal surfaces, the discrepancy between our predictions and ref 13 is too large to be explained by the different treatment of exchange/correlation. To resolve this discrepancy, we revisit the edgewise adsorption binding geometry using LDA. We apply both the VASP code,[60] with ultrasoft pseudopotentials and a plane wave basis, and the SeqQuest code,[64] which applies norm-conserving pseudopotentials and localized Gaussian basis sets. We use two different DFT packages to ensure that our predictions are not artifacts of the pseudopotentials employed. With both of these DFT codes, our predicted equilibrium Au lattice constant of 4.078 Å agrees with ref 13. However, starting with a geometry where two edge PdP protons are 1.8 Å away from surface Au atoms, PdP experiences large forces and relaxes away from the substrate. The optimized distance of closest approach between PdP protons and Au atoms is 2.36 Å, and this is associated with an adsorption energy of only 0.25 eV per PdP molecule. (The relaxed geometries are listed in the Supporting Information.) Sampling different adsorption sites by moving the PdP center of mass in the $x-y$ plane results in only small (∼0.03 eV) variations in E_{bind}.

We conclude, on the basis of the results of two very different DFT codes, that the attraction between Au(111) and edgewise adsorbed PdP is weak, of the order of 0.25 eV within the LDA approximation, not the ∼10 eV reported previously.[13] Note that a DFT work which adopts the edgewise adsorption geometry of ref 13 to study PdP on Al(111) also reported a LDA binding energy of a small fraction of an electronvolt.[14]

We emphasize that this 0.25 eV attractive interaction is computed using LDA. In the remainder of this work, we will use PBE or DFT+U based on PBE. The PBE exchange correlation functional predicts a negligible binding energy between an edgewise-adsorbed PdP tube on Au(111).

2. Flat Adsorption Geometry. Next, we examine a flat adsorption geometry. We place the center of mass of the PdP molecule, namely the Pd atom, atop the hollow, bridge, and

(90) For a recent review, see: Shelnutt J. A. In *The Porphyrin Handbook*; Kadish, K. M., Smith, K. M., Guilard, R., Eds.; Academic Press: San Diego, 2000; Vol. 7, p 167.
(91) Haddad, R. E.; Gazeau, S.; Pécaut, J.; Marchon, J.-C.; Medforth, C. J.; Shelnutt, J. A. *J. Am. Chem. Soc.* **2003**, *205*, 1253.

Table 2. Flat Adsorption Geometry PdP Binding Energies on Various Au(111) Surface Sites and Some Intramolecular Distances: Metal−Nitrogen (d_N), Metal−Porphine Ring (d_p), Metal−Gold Surface (d_{Au}), and Porphine−Gold Surface ($d_{p/Au}$)[a]

site	E_{bind}	d_N	d_p	d_{Au}	$d_{p/Au}$
top	−0.270	2.040	−0.079	3.40	3.48
bridge	−0.267	2.039	−0.079	3.40	3.48
hollow	−0.255	2.039	−0.064	3.39	3.45

[a] Calculations are performed using three layers of Au atoms and Γ-point sampling. Energies and distances are in units of eV and Å, respectively.

top sites of the Au(111) surface and carry out geometry optimization. Γ-point sampling and the three-layer, 90-atom Au(111) supercell described previously are used. Due to the weak interaction between PdP and Au(111), geometric relaxation along the *z* direction is slow. Nevertheless, when PdP previously optimized in the gas phase is initially placed 3.17 Å from the top layer of Au(111) atoms, the porphine ring eventually relaxes to a distance ∼3.5 Å above the gold surface. Here, the *z* coordinate of the top layer of the gold substrate is averaged over all atoms in that layer, and the porphine ring *z*-position is averaged over all porphine atoms other than Pd.

The binding energies for all three sites are similar, between 0.255 and 0.270 eV (Table 2). They are consistent with a weak, non-site-specific van der Waals interaction between PdP and Au(111). There are minimal changes in the PdP geometry compared to that in the gas-phase system, with the Pd−N distance expanding by less than 0.01 Å and the Pd(II) ion displacing toward the gold substrate by less than 0.1 Å. PBE underestimates van der Waals forces between PdP and Au. For a qualitative comparison, our molecular force field calculation[78] yields a 0.54 eV binding energy for bare porphine (H_2P) molecules adsorbed in a flat geometry on Au(111). Increasing the number of gold layers from three to four increases the PBE E_{bind} by only 0.005 eV, showing that the calculation is adequately converged with respect to the system size employed.

The absence of PdP−Au(111) covalent bonding is confirmed by examining the electron density distributions and the electronic density of states (DOS). The electron densities associated with PdP and the Au surface presented in Figure 3a show minimal overlap. Figure 3b superimposes the DOS of an isolated PdP (inverted curve in the upper half of the figure) with that of the adsorbed PdP−Au(111) complex (lower curve). We align the two sets of DOS by performing calculations where PdP is moved far from the Au(111) surface, and we then line up the lowest occupied orbitals, namely the Pd 4p states. We find that a 6 or 8 Å separation is sufficient to converge the DOS alignment to the infinite separation limit. The DOSs show that the Fermi level of the PdP−Au complex resides within the highest/lowest occupied molecular orbital gap of PdP, far from PdP d-orbital levels. Thus, we do not expect any charge transfer between PdP and Au. Figure 3b also depicts the orbitals in isolated PdP and the PdP−Au complex which exhibit substantial Pd 4d character. There are more than five such states because of hybridization between the Pd and nitrogen orbitals. The highest 4d-dominated state is unoccupied, consistent with the $4d^8$ Pd(II) electronic configuration. Adsorbing PdP on to Au(111) perturbs these Pd 4d-like orbitals by only a small fraction of an electronvolt, and their occupancies do not change.

To summarize, using the PBE exchange correlation functional, we find that PdP lies flat on the Au(111) surface, with a binding energy of 0.27 eV. It does not adsorb in an edgewise geometry. This conclusion is in qualitative agreement with experimental observation of substituted porphyrins lying flat on gold surfaces.[6,10−12] The interaction is dominated by van der Waals forces and is not surface site specific.

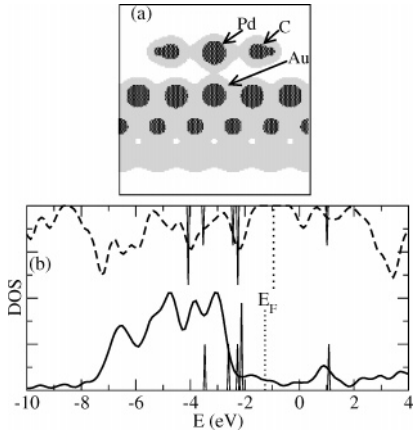

Figure 3. (a) Distribution of electron density in a *y*-cross-sectional plane through the Pd atom. Light (dark) shaded regions denote densities of at least 0.1 (1.0) electron/Å^3. (b) Electronic density of states for palladium porphine (PdP) adsorbed at the Au(111) top site. The solid and (inverted) dashed curves depict the DOS of the PdP−Au complex and of an isolated PdP molecule, respectively, broadened by Gaussians of width 0.1 eV. The sharp lines depict contributions from orbitals which have substantial Pd 4d character. The Fermi levels (E_F) are shown as dotted lines.

Table 3. Flat Adsorption Geometry Binding Energies (eV), Total Spin Magnetic Moment in the Supercell (μ_B), and Geometries of MnP, Mn(H_2O)P, and MnClP Adsorbed at Various Au(111) Sites[a]

site	E_{bind}	m	d_N	d_p	d_{Au}	$d_{p/Au}$
top	−0.800	3.77	2.010	−0.224	3.27	3.49
bridge	−0.740	3.70	2.011	−0.216	3.28	3.50
hollow	−0.680	3.68	2.014	−0.205	3.29	3.50
top (H_2O)	−0.680	3.76	2.015	+0.005	3.55	3.54
top (Cl^-)	−0.179	3.74	2.028	+0.242	3.74	3.50

[a] Distances are in Å. The PBE exchange correlation functional, four layers of Au atoms, and Γ-point Brillouin zone sampling are applied in these calculations. The symbols are described in the caption to Table 2.

D. Mn(II) Porphine on Au(111). 1. PBE Predictions. The adsorption of MnP on Au(111) is qualitatively different from that of PdP. First, we consider PBE predictions using four Au layers and Γ-point sampling. While PBE does not predict the correct MnP high-spin ground state, we will show that it yields qualitatively correct trends for MnP adsorbed on Au(111) in the absence of an electric field. Since DFT+U calculations are more expensive than PBE, it is also more convenient to use the latter for convergence tests with respect to system size.

Table 3 shows that the PBE binding energies for MnP on Au(111) are significantly larger than for PdP, and they are more site-specific. The top, bridge, and hollow site E_{bind} differ by up to 0.12 eV. The optimized geometries indicate that Mn ion is displaced out of the porphine plane toward the gold surface by more than 0.2 Å. On the other hand, the porphine ring remains ∼3.5 Å from the gold surface, demonstrating that the stronger attraction arises from the Mn ion interacting with the gold substrate. The magnitude of the out-of-plane Mn displacement toward Au(111) correlates with increasing binding energy as the adsorption site varies. When a H_2O ligand is bound to the Mn ion at the top site, the Mn ion becomes almost coplanar with the porphine ring, and E_{bind} is slightly reduced, to a value

Table 4. Convergence of MnP Binding Energy (eV) and Spin Magnetic Moments (μ_B) at the Top Site of Au(111) as the Number of Au Layers and Brillouin Zone Sampling Vary

Au layers	*k*-point	E_{bind}	*m*
3	1 × 1 × 1	−0.869	3.83
3	2 × 2 × 1	−0.688	3.19
3	3 × 3 × 1	−0.727	3.58
4	1 × 1 × 1	−0.800	3.77
4	2 × 2 × 1	−0.783	3.79
5	1 × 1 × 1	−0.693	3.48
5	2 × 2 × 1	−0.786	3.57
6	1 × 1 × 1	−0.868	3.80

almost identical to that of the unligated MnP at the hollow site. In contrast, an isolated MnPCl is already in the Mn(III) oxidiation state, and its adsorption energy is drastically reduced.

Table 4 shows that four layers of gold atoms and Γ-point sampling converge the binding energy to within ∼0.09 eV. E_{bind} does not converge monotonically with system size and depends on the degeneracy of the highest unoccupied orbitals of the Au(111) slab. Using Γ-point sampling, the same Fermi level degeneracy repeats itself whenever three layers of gold are added, and the E_{bind} values are almost identical for the three- and six-layer gold models. With more *k*-point sampling in the *x*−*y* directions, better convergence is obtained. We will adopt the four-layer system with Γ-point sampling as a compromise between accuracy and computational convenience. Table 4 emphasizes the importance of proper Brillouin zone sampling when treating adsorption of transition metal embedded molecules on metal surfaces. It suggests that using a finite sized, gas-phase cluster geometry to represent the gold substrate, which is always limited to Γ-point sampling and results in an electronic *insulator*, may be especially problematic.

The spin magnetic moment (*m*) of the simulation cell is also converged to ∼0.2 μ_B with four layers of Au. We have adopted the convention, frequently used in the DFT+U literature,[48,63] that reports the spin magnetic moment *m* as the difference in occupation numbers between up-spin and down-spin orbitals, in units of μ_B. The magnetic moment changes from the PBE prediction of $m = 3\ \mu_B$ for isolated MnP to $m = 3.8\ \mu_B$ for the supercell containing the adsorbed molecule. Decomposition of spin densities on atomic centers shows that the magnetic moment is localized on Mn 3d orbitals. Note that, within the framework of spin-polarized density functional theory, adding an electron to the periodically replicated gold substrate contributes zero net spin to the entire system.

In this work, we have adopted isolated ("gas phase") Mn(II)P as the reference to compare with MnP adsorbed on Au(111). Although the Mn(II) oxidation state is generally less stable in porphyrins than Mn(III), properties of stable substituted Mn(II) porphyrins have been measured,[57] and electrochemically induced transitions between Mn(II) and Mn(III) are readily realizable.[1,83] In reality, a gold electrode represents an infinite electron reservoir: when a non-ligated MnP adsorbs on a gold electrode, the final spin state, charge configuration, and molecular geometry will not be affected by the initial MnP charge state, although the binding energy measured from the Mn(III)P reference state would be different.

2. DFT+U Predictions. In this section, we apply the DFT+U technique to examine MnP adsorption at the top site of Au(111). We use four layers of Au atoms with Γ-point sampling, previously shown to yield converged E_{bind} from PBE calculations. DFT+U consistently predicts a larger E_{bind} for the top site than for the bridge site, just like the PBE exchange correlation functional.

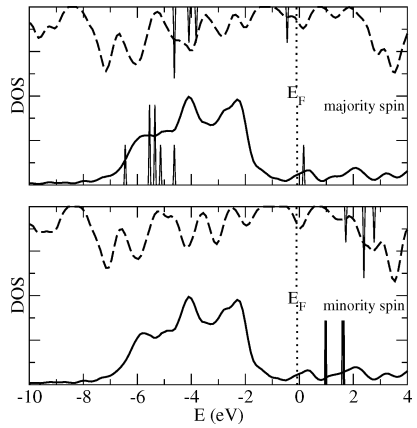

Figure 4. Same as Figure 3b, but for MnP computed using the DFT+U exchange correlation functional. The upper and lower panels refer to the majority and minority spin channels, respectively. The sharp lines are states with substantial Mn 3d character.

Table 5. Binding Energies (eV), Total Spin Magnetic Moment in the Supercell (μ_B), and Molecular Geometries of MnP and $Mn(H_2O)P$ in 0 and 0.7 V/Å Applied Field[a]

species	field	E_{bind}	*m*	d_N	d_p	d_{Au}	$d_{p/Au}$
MnP	0.000	−0.686	3.87	2.022	−0.247	3.25	3.50
MnP	0.700	−0.145	4.88	2.156	−0.540	2.94	3.48
MnP*	0.700	−0.152	3.22	2.011	−0.125	3.39	3.52
$Mn(H_2O)P$	0.000	−0.737	3.91	2.020	+0.005	3.55	3.55
Mn(Cl)P	0.000	−0.106	3.94	2.040	+0.187	3.68	3.49

[a] Distances are in Å. The DFT+U method is applied except for the case marked with the asterisk, which uses the PBE functional. The symbols and system size are described in the caption to Table 3.

Figure 4 depicts the electronic density of states in the two spin channels of both isolated MnP and the MnP−Au(111) complex. As already shown in Table 1, DFT+U (unlike PBE) yields a $m = 5\ \mu_B$ ($S = 5/2$) MnP ground state, in agreement with experiments for substituted MnP. All majority spin orbitals with substantial Mn 3d character are occupied in isolated MnP, while no such minority spin orbitals are occupied.

Adsorption of MnP on Au(111) leads to striking changes in the spectra of orbitals with substantial Mn 3d character, which are perturbed by up to 2 eV. The highest occupied majority spin Mn 3d orbital in isolated MnP is pushed into the conduction band. Overall, the MnP−Au(111) complex exhibits a magnetic moment of $m = 3.9\ \mu_B$, similar to PBE results. While both DFT+U and PBE predict similar adsorption geometries and binding energies (see Tables 3 and 5), their respective Mn 3d-like orbitals (not shown for PBE) differ in energies by up to 2 eV.

Figure 5a illustrates the charge densities in a cross-sectional *y* plane through the Mn ion and the first-layer Au atoms. In contrast to PdP (Figure 3), there is significant overlap of charge densities between Mn and the top site Au atom closest to it. On the other hand, the π-electrons on carbon atoms of MnP clearly do not interact with Au(111). Comparing the charge density of isolated MnP (Figure 5c) with that of adsorbed MnP, the top side, out-of-porphine-plane electron density in the isolated MnP is diverted to the substrate side, where it overlaps with gold orbitals.

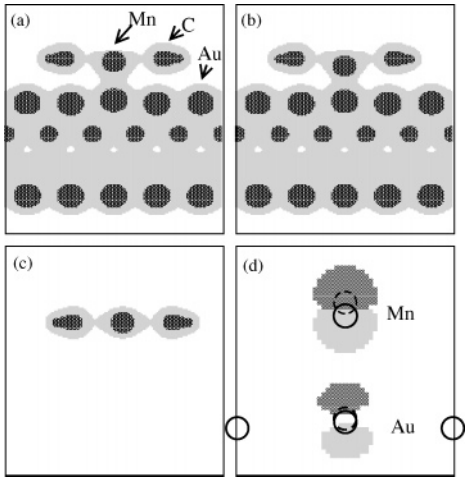

Figure 5. Distributions of electron density in a *y*-cross-sectional plane through the Mn atom, computed using the DFT+U method. (a) No applied field; (b) 0.7 eV applied field; (c) isolated MnP, zero field; (d) electron density difference between (a) and (b). In panels a, b, and c, light (dark) shaded regions denote densities of at least 0.1 (1.0) electron/Å^3. In panel d, the lighter (darker) shades depict regions of electron loss (gain) by at least 0.2 electron/Å^3 upon applying the field. The circles drawn with solid (dashed) lines donote the Mn and Au atom positions with (without) applied field. Note that these atoms and their electron clouds move in opposite directions.

To determine the extent of electron transfer between MnP and Au(111), we make a cut through the narrowest region of the funnel-shaped electron density distribution and assign charges to the two species accordingly. We find there is at most a transfer of 0.2 electron from MnP to the substrate, despite the drastic changes in the DOS and the spin multiplicity from their gas-phase values. The binding between MnP and Au(111) is thus best described as covalent or metallic.

E. Applying an Electric Potential. Given that the MnP−Au(111) interaction is associated with partial electron transfer, we expect that changing the electric potential on the gold substrate will strongly influence the adsorption behavior. An electric field which favors transfer of electrons from MnP to Au can strengthen the MnP−Au interaction. An electric field which favors electron transfer back into MnP 3d orbitals should cause the Mn(III)-like behavior to revert back to Mn(II).

Applying electric fields within plane wave density functional theory calculations has been formulated in the literature and implemented into the VASP code.[92] We apply a field of 0.7 V/Å to isolated MnP, a four-layer gold slab, and the adsorbed MnP on four layers of Au atoms. E_{bind} is obtained from the energy difference between the adsorbed and isolated systems. Γ-point sampling is used throughout.

Table 5 shows that a 0.7 V/Å electric field strongly reduces the binding energy and changes the magnetic moment to almost its isolated MnP value: $m = 4.89\ \mu_B$ according to DFT+U predictions, compared with $m = 5\ \mu_B$ in isolated MnP. The Mn−N distance, d_N, also increases from the zero-field value of 2.02 Å to 2.15 Å, which is even larger than the value of $d_N = 2.090$ Å predicted in isolated MnP. The PBE predictions for molecular geometry and spin states are substantially different; this reflects the inability of PBE to predict the correct spin state and molecular geometry for isolated MnP.

(92) Feibelman, P. J. *Phys. Rev. B* **2001**, *64*, 125403 and references therein.

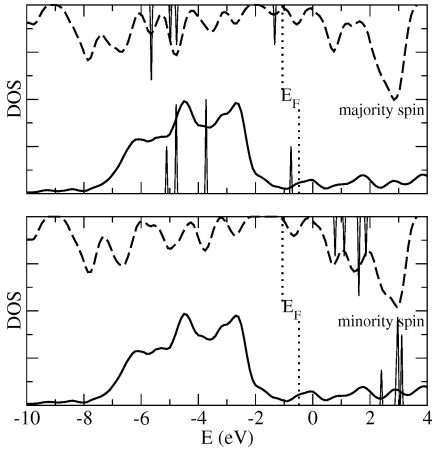

Figure 6. Same as Figure 4, for MnP computed using the DFT+U method with an applied electric field of 0.7 eV/Å.

The larger Mn−N distance in adsorbed MnP in an electric field compared to that in isolated MnP is due to the significant Mn ion displacement out of the porphine plane toward the gold substrate, and not to a change in the porphine conformation, which remains essentially planar. This is demonstrated by the similar core sizes for isolated MnP (2.090 Å) and for MnP adsorbed on Au(111) with an electric field (2.087 Å) (the core size is defined as the radius of a cylinder which can fit through the porphine hole). NSD analysis (Supporting Information) also shows that the A_{1g} (in-plane) deformation of MnP on Au(111) in the absence of an applied field is consistent with a Mn(III)-like species, with a first-order A_{1g} deformation of +0.08 Å compared to +0.11 Å predicted for isolated MnClP. As expected, with an applied electric field of 0.7 V/Å, the A_{1g} deformation of +0.31 Å is similar to that predicted for isolated MnP (+0.37 Å).

Figure 5 illustrates the effect of the applied field on the charge density. The field evidently repopulates the Mn $3d_{x^2-y^2}$-like orbital and restores electron density to the top side of the MnP molecule. There still appears substantial electron cloud overlap between MnP and the gold surface despite the small E_{bind}. Figure 5d depicts the induced charge differential. Note that the field causes both the surface top site Au atom and the Mn ion to move toward the gold substrate, whereas the electron densities on both atoms are displaced in the opposite direction.

Figure 6 plots the electronic DOS predicted by DFT+U in the applied field. Compared with the zero-field case (Figure 4), the occupied states are shifted to lower energies relative to the Fermi level. In particular, the highest lying orbital with substantial Mn 3d character is brought below the Fermi level in the MnP−Au(111) complex and is occupied by electrons. This is consistent with the field-induced change in the total magnetic moment. Nevertheless, if we demarcate the charge density at the narrowest region of the electron cloud between Au and Mn, once again we find a small, ∼0.1 electron difference between the total charge on MnP and Au with or without the electric field. Thus, while the charge and spin state of the Mn ion differ, the locus of the total electron density is not strongly affected.

The 4-layer bare gold slab is stable in the 0.7 V/Å field, and the field-induced change in its energy is proportional to the square of the field magnitude. We find that smaller, 0.525 V/Å and 0.35 V/Å electric fields lead to behavior similar to that

described for MnP adsorbed on gold in a 0.7 V/Å field, although the Mn−N bonds become shorter (2.109 and 2.102 Å, respectively). Due to the technical difficulty of converging a DFT+U calculation in a system with spin polarization, a zero band gap, and an electric field, we have not located the minimal field needed to trigger this switching. This will be investigated in a future work. These calculations are performed in vacuum, and we have not attempted to relate the field strength to an electrostatic potential. In electrochemical cells, where the molecules and electrodes are immersed in electrolytes, the voltage difference required to reduce Mn(III) porphyrins to Mn(II) is small: about 0.4 V in water[83] and on the order of 0.2−0.3 V in organic solvents.[1]

IV. Conclusions

In this work, we use a combination of density functional theory (DFT) in the generalized gradient approximation (GGA) and the DFT+U technique to study the adsorption of transition metal porphine molecules on atomistically flat Au(111) substrates. The PBE exchange correlation functional is adequate for treating palladium porphine (PdP). We find that PdP preferentially adsorbs flat on Au(111) surfaces, in agreement with experimental observations of substituted porphyrins lying flat on gold surfaces.[6,10−12] The binding energy is 0.27 eV, irrespective of the adsorption site. There is no charge transfer or covalent bonding between PdP and Au, and the interaction is predominantly dispersive. In contrast to the results of a previous DFT calculation,[13] we find that a self-assembled tube-like geometry with the PdP adsorbing edgewise on Au(111) is not energetically favorable. Using multiple DFT codes and types of pseudopotentials, we find that the LDA binding energy for this edgewise adsorption geometry is 0.25 eV, not ∼10 eV as previously predicted.[13] The PBE exchange correlation functional predicts little or no binding. Furthermore, an accurate binding energy for this geometry requires more extensive Brillouin zone sampling than has been attempted previously.

The behavior of manganese porphine (MnP) is qualitatively different. The PBE exchange correlation functional does not reproduce the correct ground state (high-spin $S = 5/2$ state) or the experimental Mn−nitrogen distance. However, PBE can be augmented with the DFT+U technique, which can be parametrized to yield the correct ordering of spin multiplicity. The DFT+U ground-state geometry exhibits a Mn−N distance in good agreement with experiments and B3LYP predictions.

MnP selectively binds to the top site of Au(111). When we use Mn(II)P as the reference state, the binding energy of MnP on Au(111) is significantly larger than for PdP. The adsorbed MnP exhibits partial charge transfer from orbitals with substantial Mn 3p character to Au(111) states. The overall magnetic moment also changes from $m = 5\ \mu_B$ ($S = 5/2$) to $m \approx 4\ \mu_B$ ($S = 2$). In other words, Mn takes on a 3+ oxidiation state character.

This MnP−Au(111) interaction can be partially reversed by applying an electric field with the appropriate polarity. A sufficiently large field causes the Mn ion to revert back to a Mn(II)-like spin state, resulting in a significant, up to 0.13 Å, increase in the Mn−N distance within the porphine ring. This suggests that appropriately substituted Mn porphyrins deposited on gold electrodes may be useful for demonstrating electric-field-triggered conformational changes that are potentially pertinent to harvesting nanomechanical work and selective ligand binding.[16]

In summary, we have successfully applied the DFT+U technique to transition metal ions in a condensed-phase environment with fully periodic boundary conditions. With this approach, the energy difference between the spin states can be parametrized using not just B3LYP, which gives qualitatively correct spin orderings for many manganese complexes, but experimental data, quantum chemistry methods, and quantum Monte Carlo calculations as well. As such, this versatile technique can potentially be used for general, accurate, all-DFT-based treatment of transition metal ions in aqueous systems, water−material interfaces, and biological environments.[33,55]

Acknowledgment. We thank John Shelnutt, Peter Feibelman, Rick Muller, Richard Martin, Kevin Zavadil, and Donald Truhlar for useful suggestions. This work was supported by the Department of Energy under Contract DE-AC04-94AL85000. Sandia is a multiprogram laboratory operated by Sandia Corporation, a Lockheed Martin Company, for the U.S. Department of Energy. V.S.B. acknowledges supercomputer time from the National Energy Research Scientific Computing (NERSC) center and financial support from the National Science Foundation (NSF) Career Program, Award CHE 0345984, and the NSF Nanoscale Exploratory Research (NER), Award ECS 0404191.

Supporting Information Available: Description of the DFT+U implementation; LDA-predicted coordinates of PdP, Au(111) slab, and PdP adsorbed edgewise on Au(111); normal-coordinate structure decomposition (NSD) analyses for some computed structures and crystal structures; complete citation for ref 74. This material is available free of charge via the Internet at http://pubs.acs.org.

JA056630O